Large-pore Layered Networks, Polycatenated Frameworks and Three-dimensional Frameworks of Uranyl Tri(biphenyl)amine/Tri(phenyl)amine Tricarboxylate: Solvent/Ligand-dependent Dual Regulation

Shuai Wang,[†,‡,#] Lei Mei, [‡,#] Ji-pan Yu,[‡,#] Kong-qiu Hu, [‡] Zhi-rong Liu,[†] Zhi-fang Chai [‡,&] and Wei-qun Shi*,[‡]*

[†] School of Nuclear Science and Engineering, East China University of Technology, Nanchang, 330013, China

[‡] Laboratory of Nuclear Energy Chemistry, Institute of High Energy Physics, Chinese Academy of Sciences, Beijing 100049,China

[&] School of Radiological and Interdisciplinary Sciences and Collaborative Innovation Center of Radiation Medicine of Jiangsu Higher Education Institutions, Soochow University, Suzhou 215123, China

Supplementary Information

Table of contents

Figure S3. The tritopic **L2** linkers undergo remarkable changes from a nearly flat conformation to a distorted non-coplanar conformation and result in a 3D framework with a (10, 3)-connected topology, which contains a helical chain viewed along *a* axis.

Figure S4. a) Strong hydrogen-bonding capacity of water molecules for promoting the formation of helical chains and subsequent interpenetration for **4**; b-c) crystal-lattice water molecules (O2W) located near phenyl moieties might induce the rotation of phenyl moiety around C-C bond axis and final the deflection of molecular topological structure; d-e) crystal-lattice water molecules (O1W) promote the formation and stabilization of two-fold interpenetrating networks through hydrogen-bonding to terminal oxygen atoms of uranyl centers from adjacent helical chains of **4**.

Figure S5. Simulated and experimental PXRD patterns for **1**.

Figure S6. Simulated and experimental PXRD patterns for **3**.

Figure S7. Simulated and experimental PXRD patterns for **4**.

Figure S8. IR spectrum of compound **1**.

Figure S9. IR spectrum of compound **3**.

Figure S10. IR spectrum of compound **4**.

Figure S11. Thermogravimetric analysis of compound **1**.

Figure S12. Thermogravimetric analysis of compound **3**.

Figure S13. Thermogravimetric analysis of compound **4**.

S2. Tables

Table S1. Selected bond distances (Å) and angles (deg) of uranyl compounds **1-4**.

S1. Typical Figures

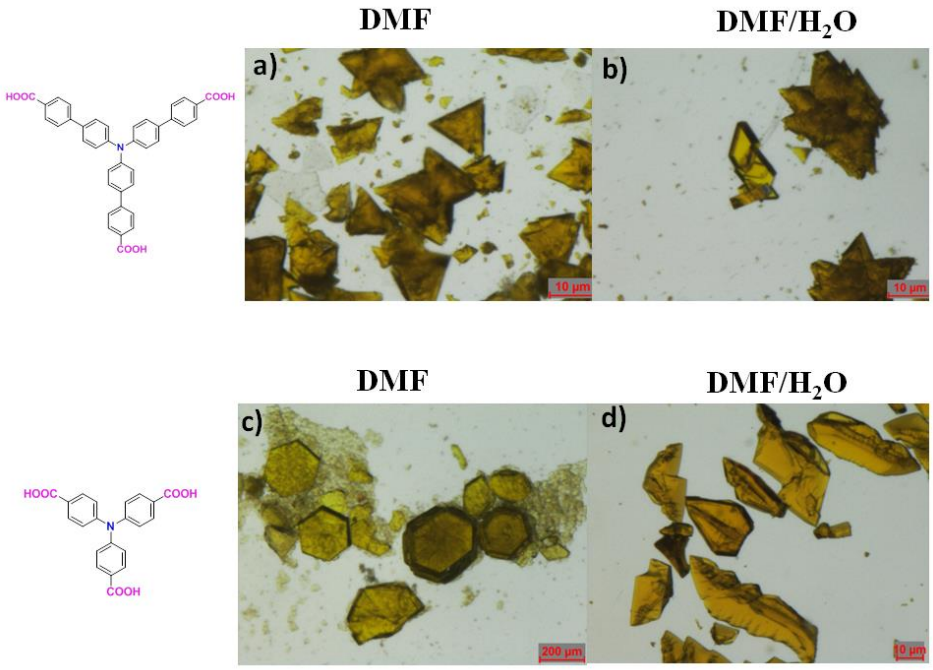

Figure S1. The optical photographs of **1**-**4** synthesized in DMF or DMF/H_2O systems.

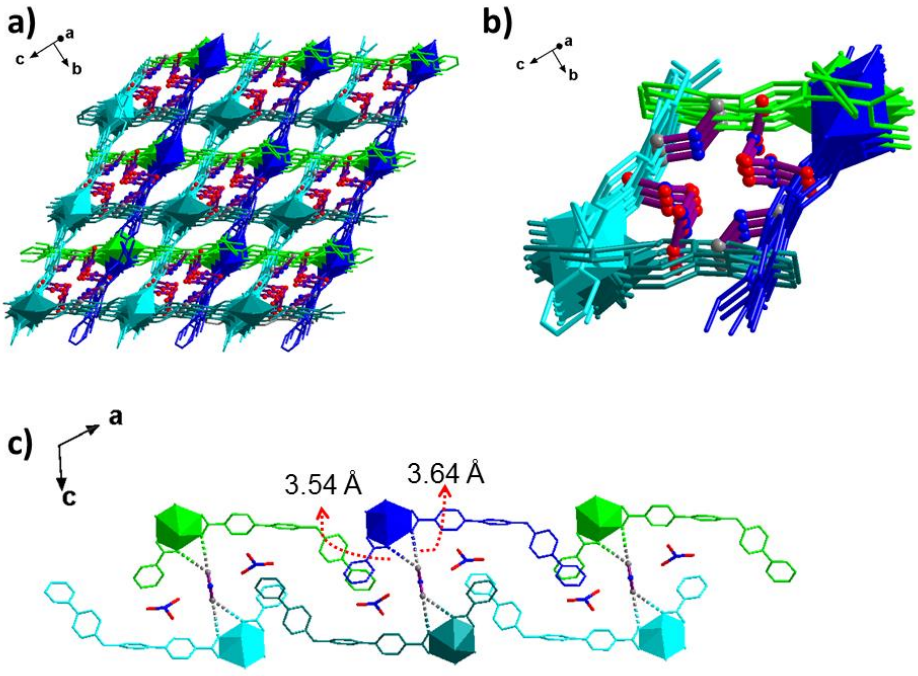

Figure S2. a) Polycatenated framework of 2 with free dimethylammonium ($[NH_2(CH_3)_2]^+$) cations and nitrate (NO_3^-) anions; b) dimethylammonium ($[NH_2(CH_3)_2]^+$) cations and nitrate (NO_3^-) anions located at the quadrilateral channels with both side lengths of 6.42 Å; c) weak interactions (C($[NH_2(CH_3)_2]^+$)---O(carboxyl): 3.54 Å and 3.64 Å) between $[NH_2(CH_3)_2]^+$ cations and adjacent uranyl centers.

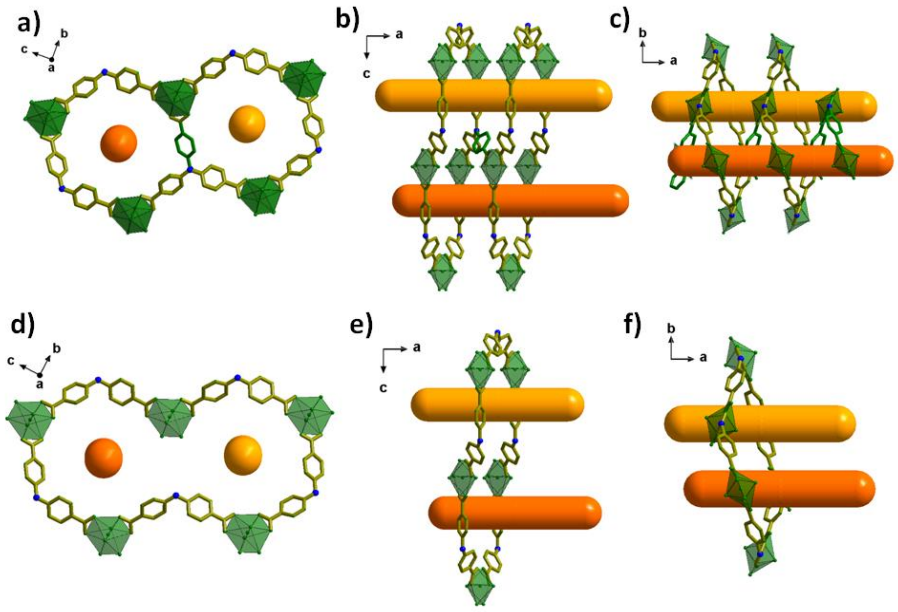

Figure S3. The tritopic **L2** linkers undergo remarkable changes from a nearly flat conformation to a distorted non-coplanar conformation and result in a 3D framework with a (10, 3)-connected topology, which contains a helical chain viewed along *a* axis.

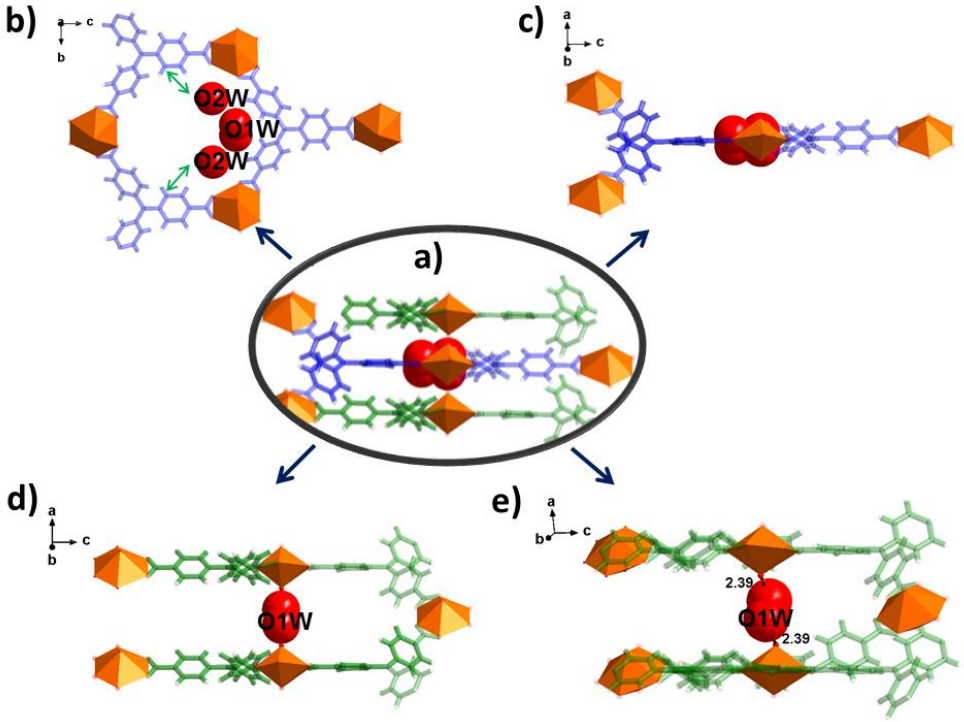

Figure S4. a) Strong hydrogen-bonding capacity of water molecules for promoting the formation of helical chains and subsequent interpenetration for **4**; b-c) crystal-lattice water molecules (O2W) located near phenyl moieties might induce the rotation of phenyl moiety around C-C bond axis and final the deflection of molecular topological structure; d-e) crystal-lattice water molecules (O1W) promote the formation and stabilization of two-fold interpenetrating networks through hydrogen-bonding to terminal oxygen atoms of uranyl centers from adjacent helical chains of **4**.

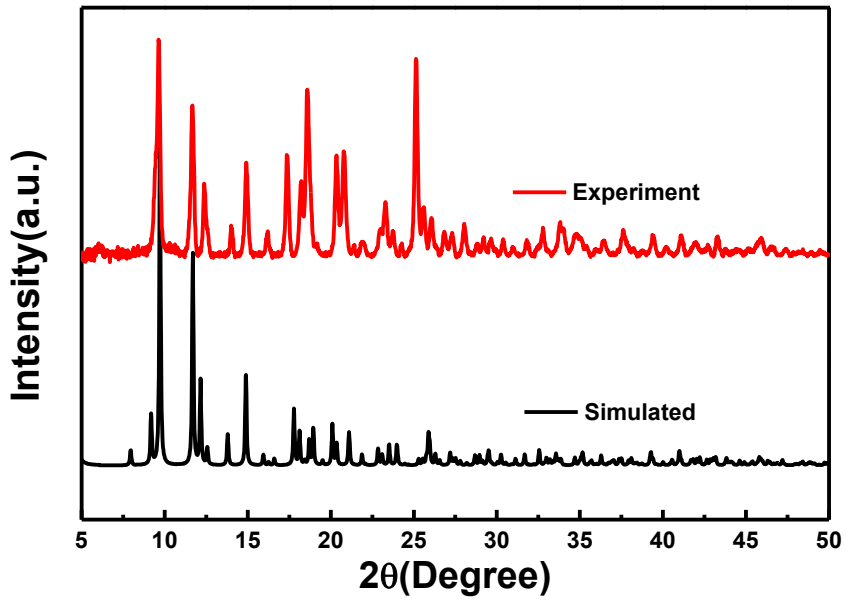

Figure S5. Simulated and experimental PXRD patterns for **1**.

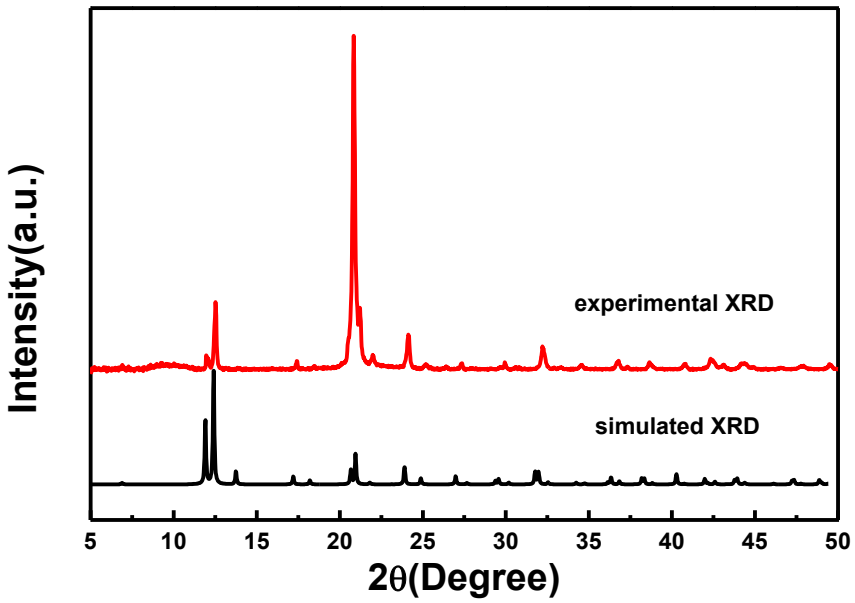

Figure S6. Simulated and experimental PXRD patterns for **3**.

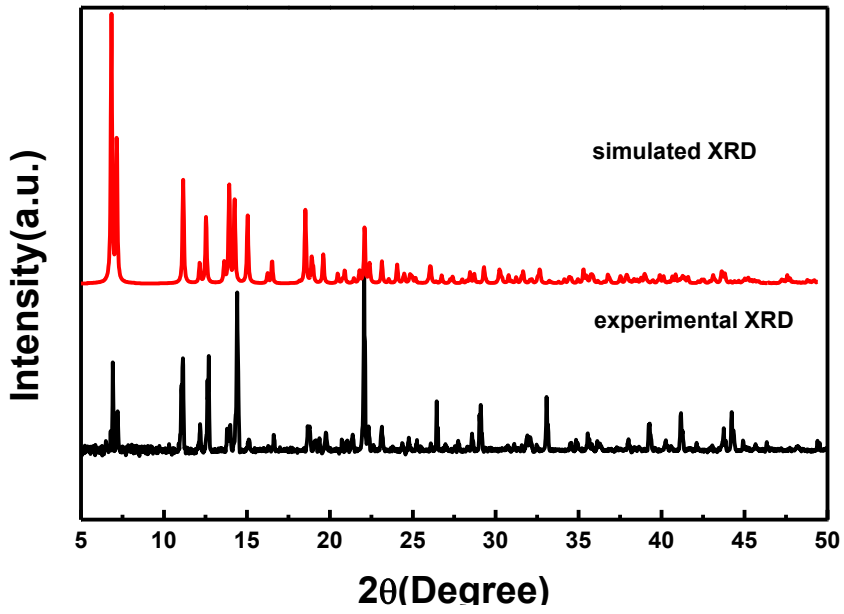

Figure S7. Simulated and experimental PXRD patterns for **4**.

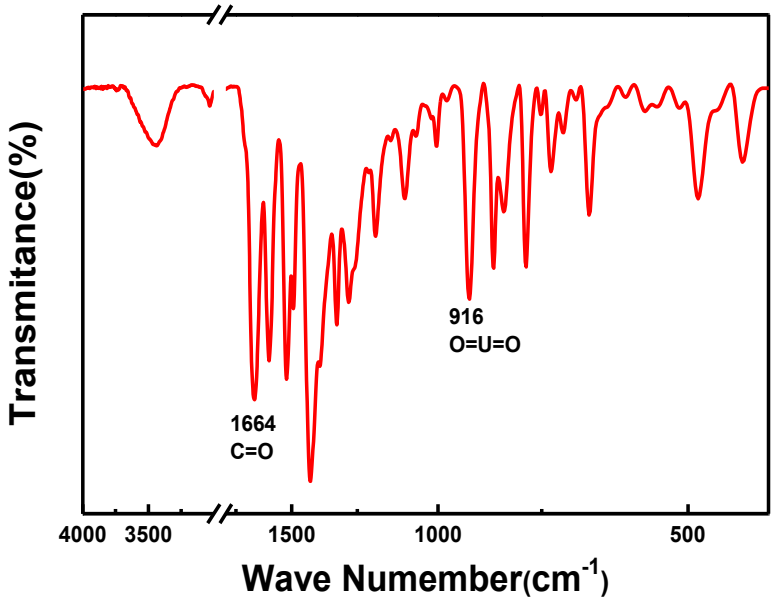

Figure S8. IR spectrum of compound **1**.

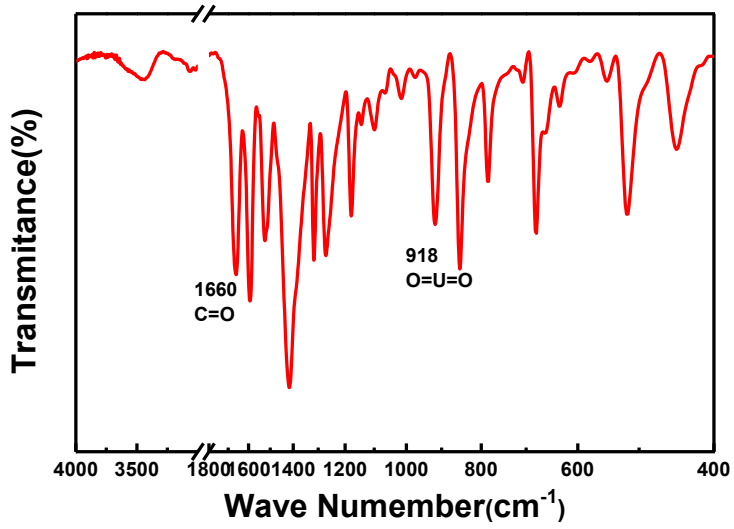

Figure S9. IR spectrum of compound **3**.

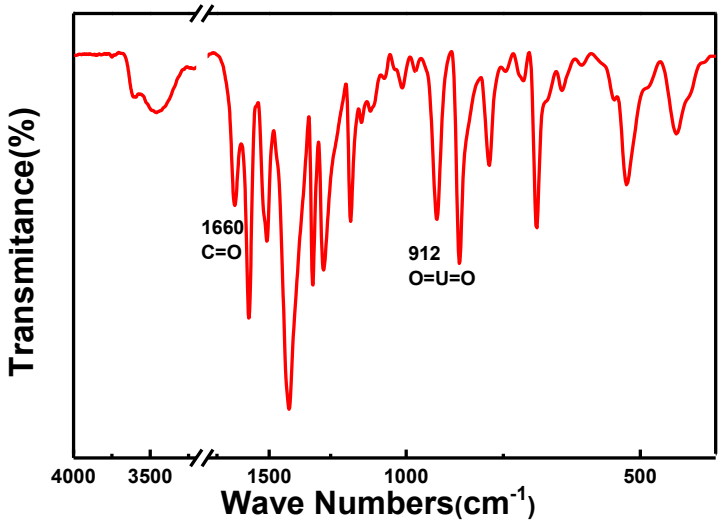

Figure S10. IR spectrum of compound **4**.

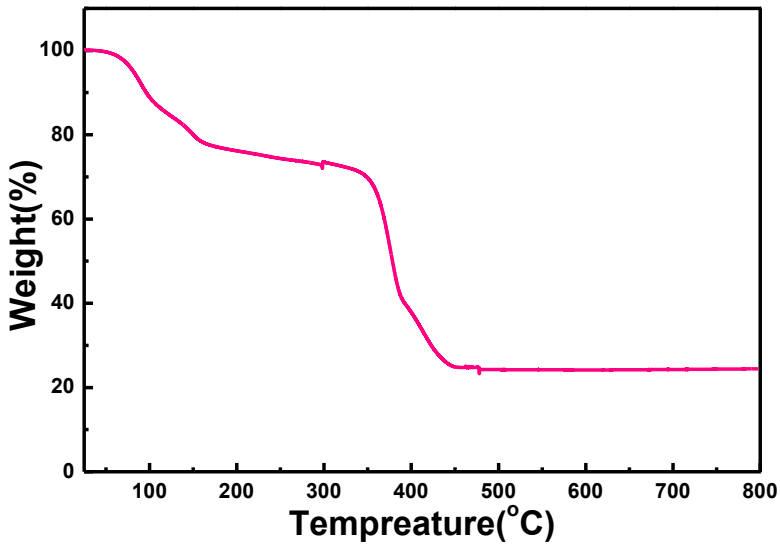

Figure S11. Thermogravimetric analysis of compound **1**.

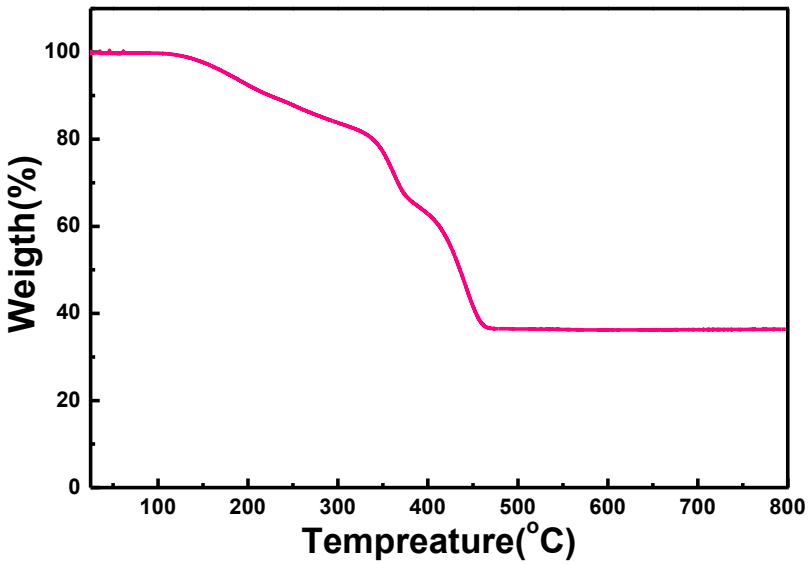

Figure S12. Thermogravimetric analysis of compound **3**.

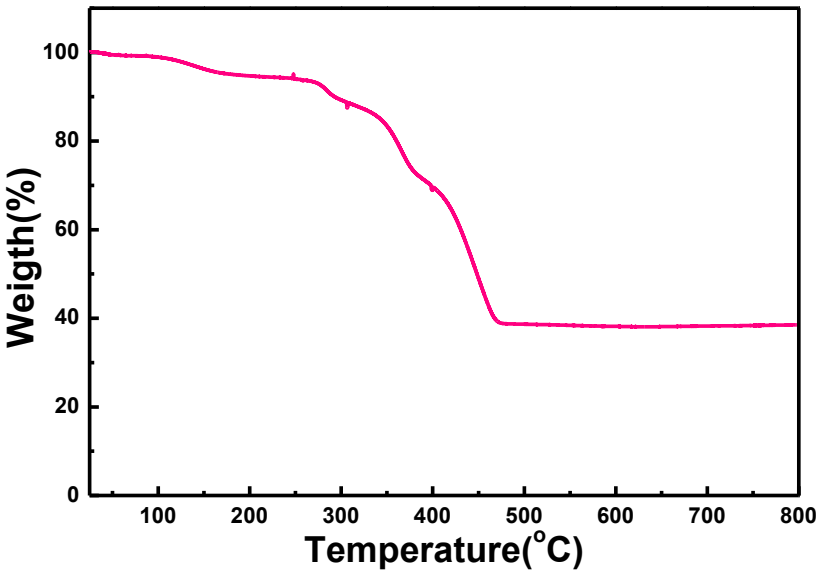

Figure S13. Thermogravimetric analysis of compound **4**.

S2. Tables

Table S1. Selected bond distances (Å) and angles (deg) of uranyl compounds **1-4**.

		1	
U(1)-O(4)	1.69(2)	U(1)-O(2)	2.47(2)
U(1)-O(3)	2.48(2)	U(1)-O(5)	2.49(3)
O(4)=U(1)=O(4')	178.8(1)		
		2	
U(1)-O(3)	1.763(18)	U(1)-O(4)	1.645(18)
U(1)-O(1)	2.437(14)	U(1)-O(2)	2.439(13)
U(1)-O(5)	2.497(14)	U(1)-O(6)	2.452(13)
U(1)-O(7)	2.434(12)	U(1)-O(8)	2.514(13)
O(3)=U(1)=O(4)	179.2(7)		
		3	
U(1)-O(1)	1.729(18)	U(1)-O(2)	2.447(10)
O(1)=U(1)=O(1')	180.0(0)		
		4	
U(1)-O(1)	1.711(11)	U(1)-O(2)	2.471(7)
U(1)-O(3)	2.466(7)	U(1)-O(4)	2.444(7)
O(1)=U(1)=O(1')	179.1(6)		